HHS Public Access

Author manuscript

Magn Reson Med. Author manuscript; available in PMC 2019 March 01.

Published in final edited form as:

Magn Reson Med. 2018 March ; 79(3): 1595–1601. doi:10.1002/mrm.26776.

Gradient nonlinearity effects on upper cervical spinal cord area measurement from 3D T1-weighted brain MRI acquisitions

Nico Papinutto[1,*], **Rohit Bakshi**[2], **Antje Bischof**[1], **Peter A. Calabresi**[3], **Eduardo Caverzasi**[1], **R. Todd Constable**[4], **Esha Datta**[1], **Gina Kirkish**[1], **Govind Nair**[5], **Jiwon Oh**[3,6], **Daniel Pelletier**[7], **Dzung L. Pham**[8], **Daniel S. Reich**[5], **William Rooney**[9], **Snehashis Roy**[8], **Daniel Schwartz**[9], **Russell T. Shinohara**[10], **Nancy L. Sicotte**[11], **William A. Stern**[1], **Ian Tagge**[9], **Shahamat Tauhid**[2], **Subhash Tummala**[2], and **Roland G. Henry**[1,12] **for the North American Imaging in Multiple Sclerosis Cooperative**[13]

[1]Department of Neurology, University of California San Francisco

[2]Department of Neurology, Brigham and Women's Hospital

[3]Department of Neurology, The Johns Hopkins University

[4]Yale University, School of Medicine

[5]Translational Neuroradiology Section, National Institute of Neurological Disorders and Stroke

[6]Department of Neurology, University of Toronto

[7]Department of Neurology, University of Southern California

[8]Center for Neuroscience and Regenerative Medicine, Henry M. Jackson Foundation

[9]Advanced Imaging Research Center, Oregon Health & Science University

[10]Department of Biostatistics, Epidemiology, and Informatics, Perelman School of Medicine, University of Pennsylvania

[11]Department of Neurology, Cedars-Sinai Medical Center

[12]Department of Radiology, University of California San Francisco

Abstract

Purpose—To explore: (1) the variability of upper cervical cord area (UCCA) measurements from volumetric brain 3D T1-weighted scans related to gradient nonlinearity (GNL) and subject positioning; (2) the effect of vendor-implemented GNL-corrections; and (3) easily applicable methods that can be used to retrospectively correct data.

Methods—A multiple sclerosis patient was scanned at 7 sites using 3T MRI scanners with the same 3D T1-weighted protocol without GNL-distortion correction. Two healthy subjects and a

[*]Corresponding author: Nico Papinutto, PhD, Department of Neurology, University of California San Francisco, 675 Nelson Rising Lane, San Francisco, CA 94158, USA, Tel: +1 415 502 7253, Fax: +1 415 353 9423, nico.papinutto@ucsf.edu.
[13]A complete list of the NAIMS participants is provided in the acknowledgment section.

This work was presented in preliminary form at the 2017 annual meeting of the Americas Committee on Treatment and Research in Multiple Sclerosis (ACTRIMS), Orlando, FL, USA, the 2017 25th annual meeting of the ISMRM and the 4th Spinal Cord MRI Workshop in Honolulu, HI, USA.

phantom were additionally scanned at a single site with varying table positions. 2D and 3D vendor-implemented GNL-correction algorithms and retrospective methods based on: (1) phantom data fit; (2) normalization with C2 vertebral body diameters; and (3) the Jacobian determinant of non-linear registrations to a template, were tested.

Results—Depending on positioning of the subject, GNL introduced up to 15% variability in UCCA measurements from volumetric brain T1-weighted scans when no distortion corrections were utilized. 3D vendor-implemented correction methods and the three proposed methods reduced this variability to less than 3%.

Conclusion—Our results raise awareness of the significant impact that GNL can have on quantitative UCCA studies and point the way to prospectively and retrospectively managing GNL-distortions in a variety of settings, including clinical environments.

Keywords

Gradient nonlinearity; upper cervical spinal cord area; spinal cord atrophy; 3D T1-weighted brain MRI acquisitions; correction algorithms

INTRODUCTION

Quantifying spinal cord atrophy in neurologic conditions from various etiologies, including trauma, inflammation, or neurodegeneration, has gained increasing attention in the neuroimaging field, particularly with the development of dedicated spinal cord imaging techniques (1–5). In multiple sclerosis (MS), upper cervical cord area (UCCA) is a surrogate of atrophy, and has been shown to be associated with physical disability, particularly in progressive stages of the disease (6–11). Spinal cord magnetic resonance imaging (MRI) remains technically challenging and adds substantial time to a scanning session, therefore many clinical sites do not routinely acquire dedicated spinal cord MRI that can provide reliable measures of UCCA. However, standard brain high-resolution 3D T1-weighted acquisitions that include the upper cervical cord can be used to provide estimates of UCCA (12,13).

Gradient nonlinearity (GNL) distortions in MRI are a consequence of technical challenges in the design of gradient coils, and an important source of systematic error interfering with the integrity of imaging metrics in longitudinal and multi-site studies. These challenges are particularly important in modern whole-body MRI scanners designed with shorter bores for increased patient comfort and reduced footprint, and fast gradient rise times for faster imaging. Moreover, a recent head-only, compact gradient design was reported to provide increased peripheral nerve stimulation thresholds (14) and very high slew rates (up to 700 T/m/s) that provide significantly improved echo-planar imaging performance (15). However, such systems have significantly increased GNL effects over standard whole-body scanners, including terms associated with asymmetric transverse gradients. Large, multisite initiatives have investigated the effect of GNL-distortions on brain tissue volume quantification (16–19); however, the effect of GNL on UCCA measurements extracted from standard brain T1-weighted acquisitions has not yet been assessed. This is extremely important, as the spinal

cord is located in the periphery of the field of view, where GNL effects are expected to introduce maximal errors.

In the present work, we explored: (1) the variability of the UCCA measurements from brain 3D T1-weighted scans related to GNL and subject positioning; (2) the effect of correction algorithms implemented on commercial scanners; and (3) easily applicable methods that can be used to retrospectively correct data acquired without optimal distortion correction.

METHODS

Image data acquisition

All human MRI acquisitions reported in the present study were conducted with the approval of Ethics Boards of the involved institutions.

MS patient acquisition: A 45-year-old male with stable relapsing-remitting MS was scanned at 7 North American Imaging in Multiple Sclerosis (NAIMS) Cooperative sites within a period of four months using Siemens 3T MRI scanners equipped with different hardware and software versions (4 Skyra, 2 Trio, 1 Verio), with the same uncorrected sagittal 3D T1-weighted MPRAGE protocol extended to the upper cervical spinal cord: voxel size=1×1×1mm^3, FOV=256×256×176mm^3, TR/TE/TI/FA=1900/2.52/900ms/9°, parallel imaging acceleration factor=2, acquisition time=4:17min. Multi-channel coils were used, with either head-neck elements (64, 20 or 12) or only head elements (32) with good sensitivity in the upper cervical cord region. The acquisition was repeated twice at each site, with repositioning.

Table position variation and distortion correction tests: To test for table position variation and distortion correction effects on UCCA measurements, two healthy controls (HC, both men, 25 and 40 years old, named HC-A and HC-B) were scanned at a single site using a Siemens 3T Skyra scanner (bore length=173cm) with the same T1-weighted protocol used for the MS patient, with a variety of table positions. Uncorrected and distortion-corrected data (using Siemens's 2D and 3D methods) were exported. Siemens methods calculate the geometric displacements from the spherical harmonic expansion of the magnetic field generated by the specific gradient coils model (17,20).

Phantom acquisition: To validate the HC acquisitions performing area measurements without confounding patient motion, a phantom manufactured in-house (a 13mm diameter cylindrical test tube filled with oil) was scanned with varying table positions using the above-mentioned T1-weighted protocol without distortion correction. The phantom was placed on the posterior elements of the head-neck coil with the main axis along the head-foot direction. A vitamin pill was placed on the side of the tube at about the position of the upper cervical cord of subjects laying in the scanner, and a water sphere was placed on top to correctly load the coil.

Healthy control acquisition on a different scanner type: To test for variability between scanners of different models, HC-B was additionally scanned twice on three Siemens 3T scanners of the same model (Trio, bore length=213cm, 40 cm longer than the

Skyra) with T1-weighted brain protocols extended to the upper cervical cord without distortion correction.

Data analysis

UCCA measurements: UCCA was measured on the brain T1-weighted acquisitions by extracting five consecutive 1mm thick axial slices perpendicular to the long axis of the cord at the C2-C3 disc level, and measuring the average area of the cord(13) using the semi-automated "cord finder toolbox" of the software JIM (version 6.0) (21) with fixed settings(22): nominal cord diameter 8mm, number of shape coefficients 24, order of longitudinal variation 12. The markers requested by the toolkit were placed at the center of the spinal cord in each of the five slices.

After having evaluated the reliability of the method on ten HC (Supporting Information), UCCA of the MS patient, HC-A and HC-B was measured by a single operator (NP)

Determination of distance between scanner isocenter and C2-C3 disc level: The C2-C3 disc distance from the scanner isocenter (Z_{CI}) was measured by determining the Z coordinate of the central slice that was extracted for the UCCA measurement for each individual (information provided by the JIM Multi-planar Reconstruction tool). If the scanner table was moved after patient positioning, the actual table position was extracted from the DICOM header and added to the Z coordinate.

Retrospective correction methods:

Phantom fit: On uncorrected acquisitions of the cylindrical phantom test tube, axial areas ($A(Z_{CI})$) were measured at the vitamin pill level as a function of Z_{CI}. $A(Z_{CI})$ was normalized to the area measured at the scanner isocenter position (A_0), and fitted to a quadratic model (least squares regression, $\varepsilon(Z_{CI})$ indicates the residual):

$$A(Z_{Cl}) / A_0 = 1 + a \times Z_{Cl} + b \times Z_{Cl}^2 + \varepsilon(Z_{Cl}) . \quad [1]$$

The estimated parameters (a,b) were used to extrapolate the UCCA measured from the uncorrected images of HC-A and HC-B to the scanner isocenter position (obtaining $UCCA_0$ for each $UCCA(Z_{CI})$).

Normalization using C2 vertebral body diameters: For all uncorrected acquisitions of HC-A, HC-B and the MS patient, the anterior-posterior and right-left diameters of the C2 vertebral body were measured with the software JIM on a single slice. $UCCA(Z_{CI})$ was divided by the product of the two diameters ($Vert(Z_{CI})$) for each acquisition.

For visual comparison with uncorrected data, a further normalization to the value measured in the acquisition with the table positioned closest to the scanner isocenter (Z_{CImin}) was performed using the equation:

$$UCCA(Z_{Cl})' = [UCCA(Z_{Cl}) / Vert(Z_{Cl})] \times Vert(Z_{Clmin}) \ , \quad [2]$$

where $UCCA(Z_{Cl})'$ indicates the normalized value.

Normalization using the Jacobian determinant of non-linear registrations: Single-subject templates were created for HC-A and the MS patient as described by Avants et al (23) using the Advanced Normalization Tools (ANTs) software package (http://stnava.github.io/ANTs). Briefly, this approach employs a non-linear, symmetric, and group-wise registration procedure that builds an optimal template representing the average shape of all images. For this step, "antsMultivariateTemplateConstruction2.sh" was run with default parameters, combining rigid (6 parameters), affine (12 parameters) and deformable registrations. Degrees of freedom in the deformable registration were equal to the number of voxels in the image times 3 (for three dimensional displacement vectors). Four levels of spatial resolution were used for each registration step. After template creation, all images were nonlinearly registered to the respective single-subject template using the SyN algorithm(24) and a cross-correlation similarity metric. The deformation field for each transformation was computed. To serve as a measure of in-plane area change, the deformation field in the Z-direction was ignored (substituting values with zeroes). The determinant of the modified Jacobian (representing the in-plane area shrinkage or expansion) was computed voxel-by-voxel. An ROI over 3 slices was drawn on the C2 vertebra on each template, and the average Jacobian of voxels within the ROI was extracted for each image. The UCCA was divided by this latter value for each image. A variant of the method can be found in Supporting Information and Supporting Figures S1 and S2.

RESULTS

Inter-site measurement variability in a single MS patient:

Across sites, the relative Z_{CI} ranged from 76mm (Z_{CImin}) to 120mm (Z_{CImax}), which corresponded to a 9.6% difference in UCCA (59.4 to 53.7mm^2) (Figure 1A). The average UCCA measured at the 7 sites was 57.2mm^2 with 2.5mm^2 standard deviation (SD). Within sites, variability in Z_{CI} with repositioning resulted in poorer rescan reproducibility (Figure 1B).

Table position variation and effect of vendor-implemented distortion correction:

A quadratic decrease in UCCA as a function of Z_{CI} was found in HC-A and HC-B scanned without distortion correction at a single site. For HC-A, the relative Z_{CI} ranged from 67 to 121mm, which corresponded to a 15.2% difference in UCCA (81.2–68.9mm^2, mean(SD)=76.1(4.2)mm^2). For HC-B (Figure 2), the relative Z_{CI} ranged from 74 to 113mm, which corresponded to a 12% difference in UCCA (81.6–71.8mm^2, mean(SD)=78.2(3.6)mm^2). The range of Z_{CI} (Z_{CImax}-Z_{CImin}) was very similar to what was observed with the single MS patient scanned across the 7 scanners, with similar corresponding relative reduction in measured UCCA.

For HC-A, vendor-implemented 2D correction decreased the difference of UCCA for extreme table positions from 15.2% to 6.8% (SD was reduced from 4.2mm^2 to 2.0mm^2). 3D correction further improved the results, reducing the difference of UCCA for extreme table positions to 2.1% (SD was reduced to 1.0mm^2). For HC-B, 2D correction decreased the difference of UCCA for extreme table positions from 12% to 5.9% (SD was reduced from 3.6mm^2 to 2.0mm^2). 3D correction reduced the difference of UCCA for extreme table positions to 1.8% (SD was reduced to 1.2mm^2) (Figure 2).

Table 1 summarizes the effect of vendor-implemented corrections together with the effect of the retrospective methods, which will be described in the subsequent sections.

Between-scanner variability for a healthy control:

HC-B was also scanned twice on 3 scanners with the longer bore. The Z_{CI} of the 6 measurements ranged from 81 to 146mm (65mm difference), which corresponded to a 9.9% difference in UCCA (82.0–73.9mm^2). For the shorter bore scanner, the Z_{CI} range was 39mm and the UCCA difference 12%. Therefore, for the longer bore scanners, a larger Z_{CI} variation was reflected in a smaller relative difference in the measured UCCA (Figure 3).

Retrospective correction methods:

Phantom fit: The fit of the phantom data was used to retrospectively correct the HC data. For HC-A (Figure 4A) the difference between UCCA measurements at extreme table positions was reduced from 15.2% to 2.9% (SD from 4.2mm^2 to 0.9mm^2) and for HC-B from 12% to 3.2% (SD from 3.6mm^2 to 1.3mm^2).

Normalization using C2 vertebral body diameters: Dividing the UCCA measurements for Vert(Z_{CI}) substantially reduced the variability with Z_{CI}, for both the HC (SD for HC-A decreased from 4.2mm^2 to 1.1mm^2 (Figure 4B), for HC-B from 3.6mm^2 to 1.9mm^2) as well as for the MS patient (from 9.6% to 1.1% for the extreme table positions, SD from 2.5mm^2 to 1.6mm^2, Figure 4D).

Normalization using the Jacobian determinant: The Jacobian normalization reduced the SD of all the UCCA measures from 4.2mm^2 to 1.1mm^2 for the HC-A (Figure 4C) and from 2.5mm^2 to 1.7mm^2 for the MS patient (Figure 4E).

DISCUSSION

In the present study, we explored the effect of GNL and subject positioning on the variability of UCCA measurements from high-resolution brain 3D T1-weighted scans.

The method used here to measure UCCA from brain scans was previously described by Liu et al (13) and applied with small variations in other spinal cord quantitative imaging studies. Although Liu and colleagues also showed that cord area measurements in a 5 mm segment, 2.5 cm below the pons, can offer a surrogate measurement for spinal cord UCCA, a measurement at the C2-C3 disc level remains the gold standard. Intra-session (test/retest) COV and inter-operator ICC of the UCCA measurements showed excellent reliability (Supporting Information), indicating that the method was appropriate for the aims of the

study. Other software to measure UCCA is available and could have been used as an alternative.

Our data showed that varying the distance from the scanner isocenter is potentially a major source of variability for UCCA estimation when using uncorrected brain 3D T1-weighted acquisitions. We found that GNL can introduce up to 15% variability in UCCA measurements, depending on subject positioning. The magnitude of the error in our study is in accordance with what was previously reported by Jovicich et al, who concluded that up to 8% error in measuring a diameter is possible at the periphery of the field of view, where GNL-distortions are strongest(17). The measure of UCCA from brain images is particularly prone to this effect, as the spinal cord is located toward the periphery of the field of view. Correctly dealing with such variability is critical for longitudinal patient monitoring studies, since it dwarfs typical clinical changes in UCCA over relevant time spans (1–2 years) (9). Defining consistent positioning with respect to the isocenter seems warranted for single-site and multi-site studies.

A quadratic decrease in UCCA as a function of Z_{CI} was found in the two HC and the phantom scanned without distortion correction at one site. We acquired data from a HC on two different 3T scanners. The effect of GNL was more pronounced for the shorter bore scanner (bore length=173cm) than for the longer bore scanner (bore length=213cm). This is consistent with the idea that stronger distortions are present in short bore scanners where technological challenges increase the difficulty in obtaining linearity in gradient performance (19).

The decrease in UCCA with Z_{CI} observed for the MS patient scanned at the 7 sites presumably reflected the combination of site-specific quadratic dependencies related to GNL, superimposed on other sources of variance in the measurement, such as subject movement and heterogeneity of hardware/software platforms reflected in different contrast-to-noise-ratio/blurring at tissue interfaces. Sites E and C used a longer bore scanner. The offset towards higher values for the UCCA measured at these sites is therefore consistent with the results obtained scanning a HC with different scanner models (Supporting Figure S3).

Even though an exhaustive exploration of correction methods available on different scanner models and vendors was beyond the scope of the present study, our data suggest that when planning to measure UCCA from standard brain high-resolution 3D T1-weighted acquisitions, 2D correction methods are suboptimal. At least for the vendor tested here, the use of 3D correction methods – introduced by this vendor about a decade ago (16,17) – is preferred. If such correction is not applied during acquisition, methods based on spherical harmonic expansion of the magnetic field could be applied off-line (17). Since this information may not be readily available from the vendors, mapping the distortion field using phantoms with fiducial markers or other complex structures is also an option to consider (19,25,26), in particular when planning a new study. However, these methods can be difficult to implement in clinical environments.

Here, we explored three different easily applicable methods that can be used to retrospectively correct data acquired with no (or suboptimal) distortion correction. The first approach was based on a quadratic fit of phantom-scan data obtained over a range of table positions. Once Eq.1 is determined from the fit, it can be applied to correct the UCCA estimated from the uncorrected images without requiring any further post-processing. Although we used a simple in-house made phantom, larger phantoms with other structures could also be used (19,25). This method is straightforward to apply, but it is not always possible to acquire phantom data with various table positions in identical hardware/software conditions used for the human data acquisitions. This is particularly true in large multi-center studies or longitudinal studies started several years in the past. As a second approach, normalization using diameters of a structure expected to be relatively stable with time and pathology (here, the C2 vertebral body) was tested. This is a powerful method for calculating % year changes in long-running longitudinal studies, as it doesn't require knowledge about distortion correction, hardware changes, or the positioning of the subject in the scanner across time points. This method gave good results for both the HC who underwent MRI at one single site and for the MS patient who was scanned at the 7 NAIMS sites. Nevertheless, this normalization can be difficult to implement and may lack precision. The C2 vertebral body, for example, is not a perfect cylinder at any level, and defining anatomical references to measure its diameters on the same plane at different time points can be challenging. Therefore this method needs to be further explored in larger datasets. We proposed a third method, based on the Jacobian determinant of non-linear registrations. This method was the most effective in reducing the GNL-related variability and it does not require further acquisitions or difficult measurements, therefore it is likely the most interesting to be implemented in typical clinical studies.

The present study has a number of limitations. First, we tested 3T scanners from a single vendor. The goal of the study was not to perform an exhaustive exploration of the extent of distortions on all possible platforms, and the results here reported would need to be extended to scanners of other manufacturers and to other magnetic field strengths. Second, the vendor-implemented correction algorithms were not exhaustively tested. Further tests are necessary to confirm our preliminary results suggesting that 3D methods are reliable, while 2D methods are suboptimal. Third, this study did not assess intensity variability due to receiver coils non-uniform sensitivity (as done by Losseff et al. (27)) that can be indirectly affected by gradient nonlinearity. Finally, solution of the problem using off-line corrections based on spherical harmonic expansion of the magnetic field was not tested. Instead, we preferred to study three practical methods that could be used in a variety of settings, including clinical environments.

CONCLUSIONS

The main goal of this technical note is to raise awareness of the significant impact that gradient nonlinearity can have in quantitative UCCA studies. While this problem is well described in the brain tissue volume quantification literature, it has not yet been addressed in spinal cord quantitative imaging. Our results point the way to managing gradient nonlinearity distortions when measuring UCCA from brain scans, taking into account the aims and the specific conditions of each study.

Supplementary Material

Refer to Web version on PubMed Central for supplementary material.

ACKNOWLEDGMENTS

• The following is a full list of individuals who contributed to this NAIMS study: Brigham and Women's Hospital, Harvard Medical School (Boston, MA): Rohit Bakshi, Renxin Chu, Gloria Kim, Shahamat Tauhid, Subhash Tummala, Fawad Yousuf; Cedars-Sinai Medical Center (Los Angeles, CA): Nancy L. Sicotte; Henry M. Jackson Foundation for the Advancement of Military Medicine (Bethesda, MD): Dzung Pham, Snehashis Roy; National Institutes of Health (Bethesda, MA): Frances Andrada, Irene C.M. Cortese, Jenifer Dwyer, Rosalind Hayden, Haneefa Muhammad, Govind Nair, Joan Ohayon, Daniel S. Reich, Pascal Sati, Chevaz Thomas; Johns Hopkins (Baltimore, MD): Peter A. Calabresi, Sandra Cassard, Jiwon Oh; Oregon Health and Science University (Portland, OR): William Rooney, Daniel Schwartz, Ian Tagge; University of California (San Francisco, CA): Antje Bischof, Eduardo Caverzasi, Esha Datta, Roland G. Henry, Gina Kirkish, Nico Papinutto, William Stern; University of Pennsylvania (Philadelphia, PA): Russell Shinohara; University of Toronto (Ontario, Canada): Jiwon Oh; Yale University (New Haven, CT): R. Todd Constable, Daniel Pelletier.

• Major support for this study was provided by the Race to Erase MS. Additional support came from RO1NS085211, R21NS093349, R01EB017255, and S10OD016356 from the National Institutes of Health, R01NS070906 and F31NS089260 from NINDS, and RG-1507–05243 from the National Multiple Sclerosis Society. The study was also partially supported by the Intramural Research Program of the National Institute of Neurological Disorders and Stroke and the Department of Defense in the Center for Neuroscience and Regenerative Medicine. The content is solely the responsibility of the authors and does not necessarily represent the official views of the funding agencies.

• The authors have no relevant disclosures.

REFERENCES

1. Castellano A, Papinutto N, Cadioli M, Brugnara G, Iadanza A, Scigliuolo G, Pareyson D, Uziel G, Kohler W, Aubourg P, Falini A, Henry RG, Politi LS, Salsano E. Quantitative MRI of the spinal cord and brain in adrenomyeloneuropathy: in vivo assessment of structural changes. Brain : a journal of neurology 2016;139(Pt 6):1735–1746. [PubMed: 27068048]
2. Israel H, Ostendorf F, Stiepani H, Ploner CJ. Spinal cord atrophy in adrenomyeloneuropathy. Archives of neurology 2005;62(7):1157. [PubMed: 16009777]
3. El Mendili MM, Cohen-Adad J, Pelegrini-Issac M, Rossignol S, Morizot-Koutlidis R, Marchand-Pauvert V, Iglesias C, Sangari S, Katz R, Lehericy S, Benali H, Pradat PF. Multi-parametric spinal cord MRI as potential progression marker in amyotrophic lateral sclerosis. PloS one 2014;9(4):e95516. [PubMed: 24755826]
4. Cohen-Adad J, El Mendili MM, Morizot-Koutlidis R, Lehericy S, Meininger V, Blancho S, Rossignol S, Benali H, Pradat PF. Involvement of spinal sensory pathway in ALS and specificity of cord atrophy to lower motor neuron degeneration. Amyotrophic lateral sclerosis & frontotemporal degeneration 2013;14(1):30–38. [PubMed: 22881412]
5. Freund P, Weiskopf N, Ward NS, Hutton C, Gall A, Ciccarelli O, Craggs M, Friston K, Thompson AJ. Disability, atrophy and cortical reorganization following spinal cord injury. Brain : a journal of neurology 2011;134(Pt 6):1610–1622. [PubMed: 21586596]
6. Bakshi R, Dandamudi VS, Neema M, De C, Bermel RA. Measurement of brain and spinal cord atrophy by magnetic resonance imaging as a tool to monitor multiple sclerosis. Journal of neuroimaging : official journal of the American Society of Neuroimaging 2005;15(4 Suppl):30S–45S. [PubMed: 16385017]
7. Lin X, Tench CR, Evangelou N, Jaspan T, Constantinescu CS. Measurement of spinal cord atrophy in multiple sclerosis. Journal of neuroimaging : official journal of the American Society of Neuroimaging 2004;14(3 Suppl):20S–26S. [PubMed: 15228756]
8. Kearney H, Miller DH, Ciccarelli O. Spinal cord MRI in multiple sclerosis--diagnostic, prognostic and clinical value. Nature reviews Neurology 2015;11(6):327–338. [PubMed: 26009002]

9. Lukas C, Knol DL, Sombekke MH, Bellenberg B, Hahn HK, Popescu V, Weier K, Radue EW, Gass A, Kappos L, Naegelin Y, Uitdehaag BM, Geurts JJ, Barkhof F, Vrenken H. Cervical spinal cord volume loss is related to clinical disability progression in multiple sclerosis. Journal of neurology, neurosurgery, and psychiatry 2015;86(4):410–418.
10. Gass A, Rocca MA, Agosta F, Ciccarelli O, Chard D, Valsasina P, Brooks JC, Bischof A, Eisele P, Kappos L, Barkhof F, Filippi M, Group MS. MRI monitoring of pathological changes in the spinal cord in patients with multiple sclerosis. The Lancet Neurology 2015;14(4):443–454. [PubMed: 25748099]
11. Rocca MA, Horsfield MA, Sala S, Copetti M, Valsasina P, Mesaros S, Martinelli V, Caputo D, Stosic-Opincal T, Drulovic J, Comi G, Filippi M. A multicenter assessment of cervical cord atrophy among MS clinical phenotypes. Neurology 2011;76(24):2096–2102. [PubMed: 21670439]
12. Liu Y, Lukas C, Steenwijk MD, Daams M, Versteeg A, Duan Y, Li K, Weiler F, Hahn HK, Wattjes MP, Barkhof F, Vrenken H. Multicenter Validation of Mean Upper Cervical Cord Area Measurements from Head 3D T1-Weighted MR Imaging in Patients with Multiple Sclerosis. AJNR American journal of neuroradiology 2016;37(4):749–754. [PubMed: 26659338]
13. Liu Z, Yaldizli O, Pardini M, Sethi V, Kearney H, Muhlert N, Wheeler-Kingshott C, Miller DH, Chard DT. Cervical cord area measurement using volumetric brain magnetic resonance imaging in multiple sclerosis. Multiple sclerosis and related disorders 2015;4(1):52–57. [PubMed: 25787053]
14. Lee SK, Mathieu JB, Graziani D, Piel J, Budesheim E, Fiveland E, Hardy CJ, Tan ET, Amm B, Foo TK, Bernstein MA, Huston J, 3rd, Shu Y, Schenck JF. Peripheral nerve stimulation characteristics of an asymmetric head-only gradient coil compatible with a high-channel-count receiver array. Magnetic resonance in medicine 2016;76(6):1939–1950. [PubMed: 26628078]
15. Tan ET, Lee SK, Weavers PT, Graziani D, Piel JE, Shu Y, Huston J, 3rd, Bernstein MA, Foo TK. High slew-rate head-only gradient for improving distortion in echo planar imaging: Preliminary experience. Journal of magnetic resonance imaging : JMRI 2016;44(3):653–664. [PubMed: 26921117]
16. Wang D, Strugnell W, Cowin G, Doddrell DM, Slaughter R. Geometric distortion in clinical MRI systems Part I: evaluation using a 3D phantom. Magnetic resonance imaging 2004;22(9):1211–1221. [PubMed: 15607092]
17. Jovicich J, Czanner S, Greve D, Haley E, van der Kouwe A, Gollub R, Kennedy D, Schmitt F, Brown G, Macfall J, Fischl B, Dale A. Reliability in multi-site structural MRI studies: effects of gradient non-linearity correction on phantom and human data. NeuroImage 2006;30(2):436–443. [PubMed: 16300968]
18. Gunter JL, Bernstein MA, Borowski BJ, Ward CP, Britson PJ, Felmlee JP, Schuff N, Weiner M, Jack CR. Measurement of MRI scanner performance with the ADNI phantom. Medical physics 2009;36(6):2193–2205. [PubMed: 19610308]
19. Caramanos Z, Fonov VS, Francis SJ, Narayanan S, Pike GB, Collins DL, Arnold DL. Gradient distortions in MRI: characterizing and correcting for their effects on SIENA-generated measures of brain volume change. NeuroImage 2010;49(2):1601–1611. [PubMed: 19682586]
20. Janke A, Zhao H, Cowin GJ, Galloway GJ, Doddrell DM. Use of spherical harmonic deconvolution methods to compensate for nonlinear gradient effects on MRI images. Magnetic resonance in medicine 2004;52(1):115–122. [PubMed: 15236374]
21. Horsfield MA, Sala S, Neema M, Absinta M, Bakshi A, Sormani MP, Rocca MA, Bakshi R, Filippi M. Rapid semi-automatic segmentation of the spinal cord from magnetic resonance images: application in multiple sclerosis. NeuroImage 2010;50(2):446–455. [PubMed: 20060481]
22. Papinutto N, Schlaeger R, Panara V, Caverzasi E, Ahn S, Johnson KJ, Zhu AH, Stern WA, Laub G, Hauser SL, Henry RG. 2D phase-sensitive inversion recovery imaging to measure in vivo spinal cord gray and white matter areas in clinically feasible acquisition times. Journal of magnetic resonance imaging : JMRI 2015;42(3):698–708. [PubMed: 25483607]
23. Avants BB, Yushkevich P, Pluta J, Minkoff D, Korczykowski M, Detre J, Gee JC. The optimal template effect in hippocampus studies of diseased populations. NeuroImage 2010;49(3):2457–2466. [PubMed: 19818860]
24. Avants BB, Epstein CL, Grossman M, Gee JC. Symmetric diffeomorphic image registration with cross-correlation: evaluating automated labeling of elderly and neurodegenerative brain. Medical image analysis 2008;12(1):26–41. [PubMed: 17659998]

25. Tao S, Trzasko JD, Gunter JL, Weavers PT, Shu Y, Huston J, Lee SK, Tan ET, Bernstein MA. Gradient nonlinearity calibration and correction for a compact, asymmetric magnetic resonance imaging gradient system. Physics in medicine and biology 2017;62(2):N18–N31. [PubMed: 28033119]

26. Wang D, Doddrell DM, Cowin G. A novel phantom and method for comprehensive 3-dimensional measurement and correction of geometric distortion in magnetic resonance imaging. Magnetic resonance imaging 2004;22(4):529–542. [PubMed: 15120173]

27. Losseff NA, Webb SL, O'Riordan JI, Page R, Wang L, Barker GJ, Tofts PS, McDonald WI, Miller DH, Thompson AJ. Spinal cord atrophy and disability in multiple sclerosis. A new reproducible and sensitive MRI method with potential to monitor disease progression. Brain : a journal of neurology 1996;119 (Pt 3):701–708. [PubMed: 8673483]

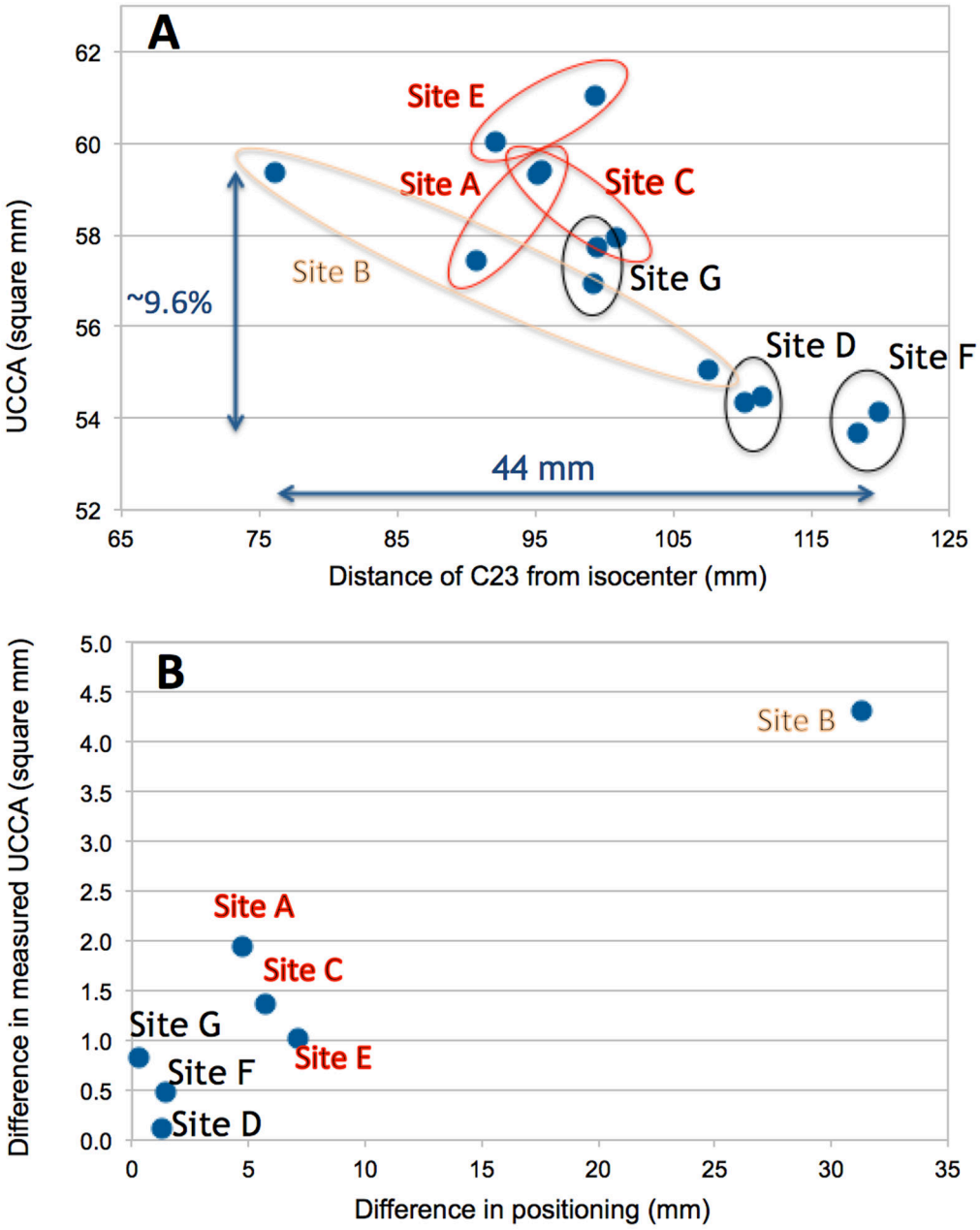

Figure 1.

A: UCCA of the multiple sclerosis patient measured at the 7 NAIMS sites as a function of the distance between the C2-C3 disc and the scanner isocenter (Z_{CI}). B: Within sites variability in Z_{CI} with repositioning was associated with poorer rescan reproducibility.

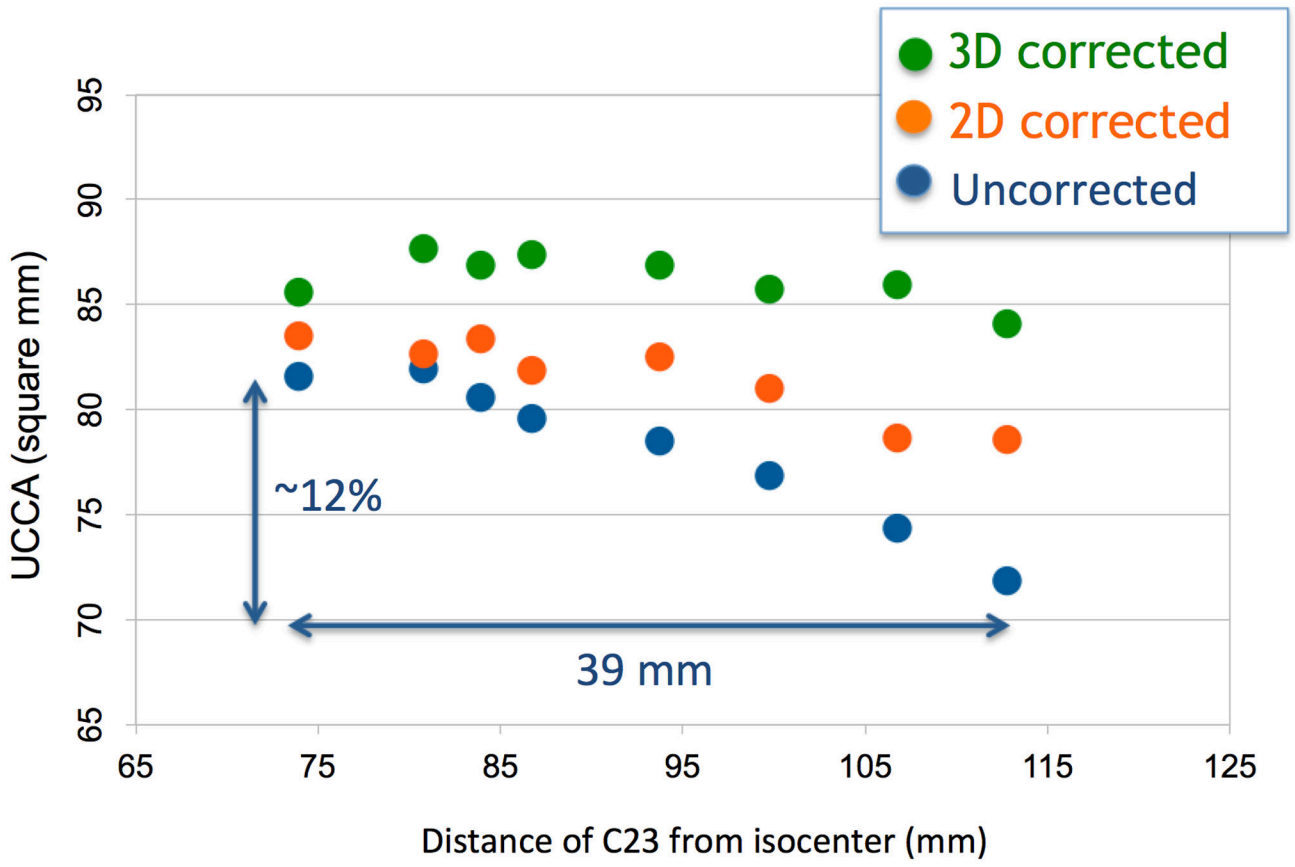

Figure 2.
UCCA as a function of the distance of the C2–3 disc from scanner isocenter for a healthy control: uncorrected and distortion-corrected data.

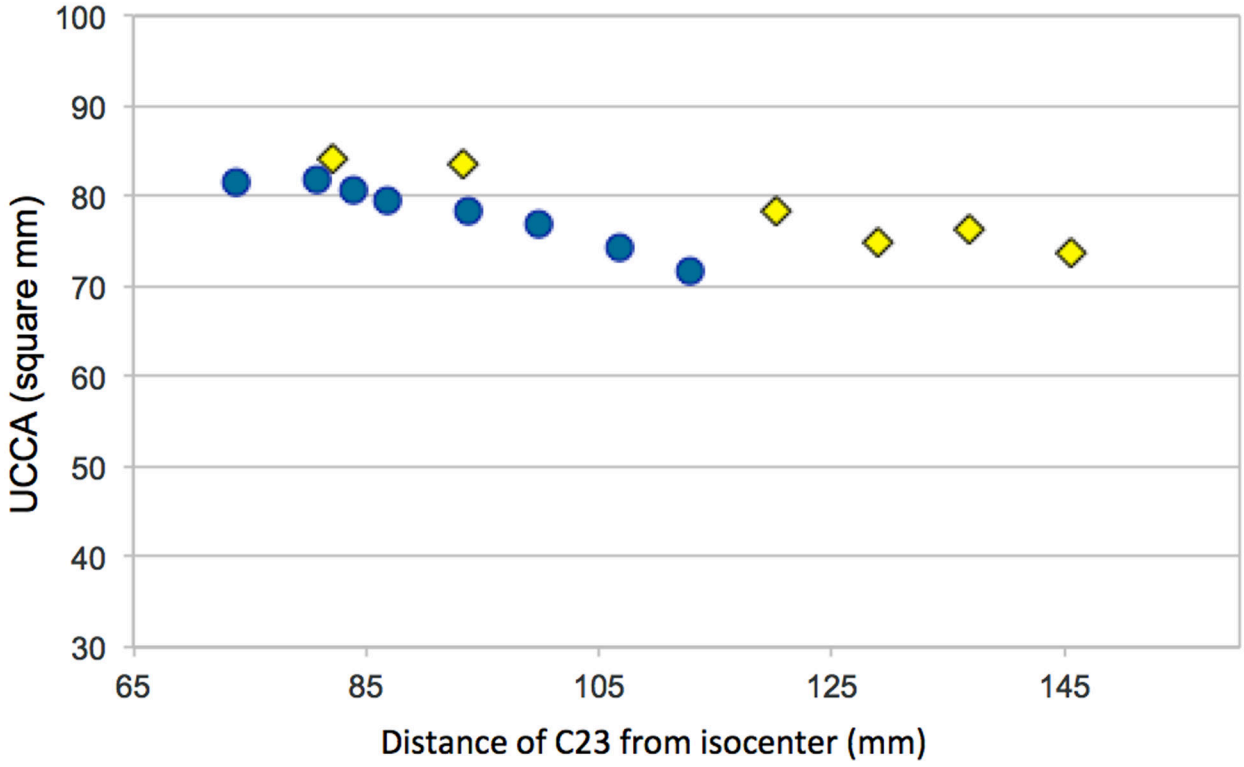

Figure 3.
UCCA measured in the same healthy control scanned on a Skyra (bore length=173cm, blue dots) and on 3 different Trio scanners (bore length=213cm, yellow diamonds), as a function of the distance of the C2–3 disc from scanner isocenter.

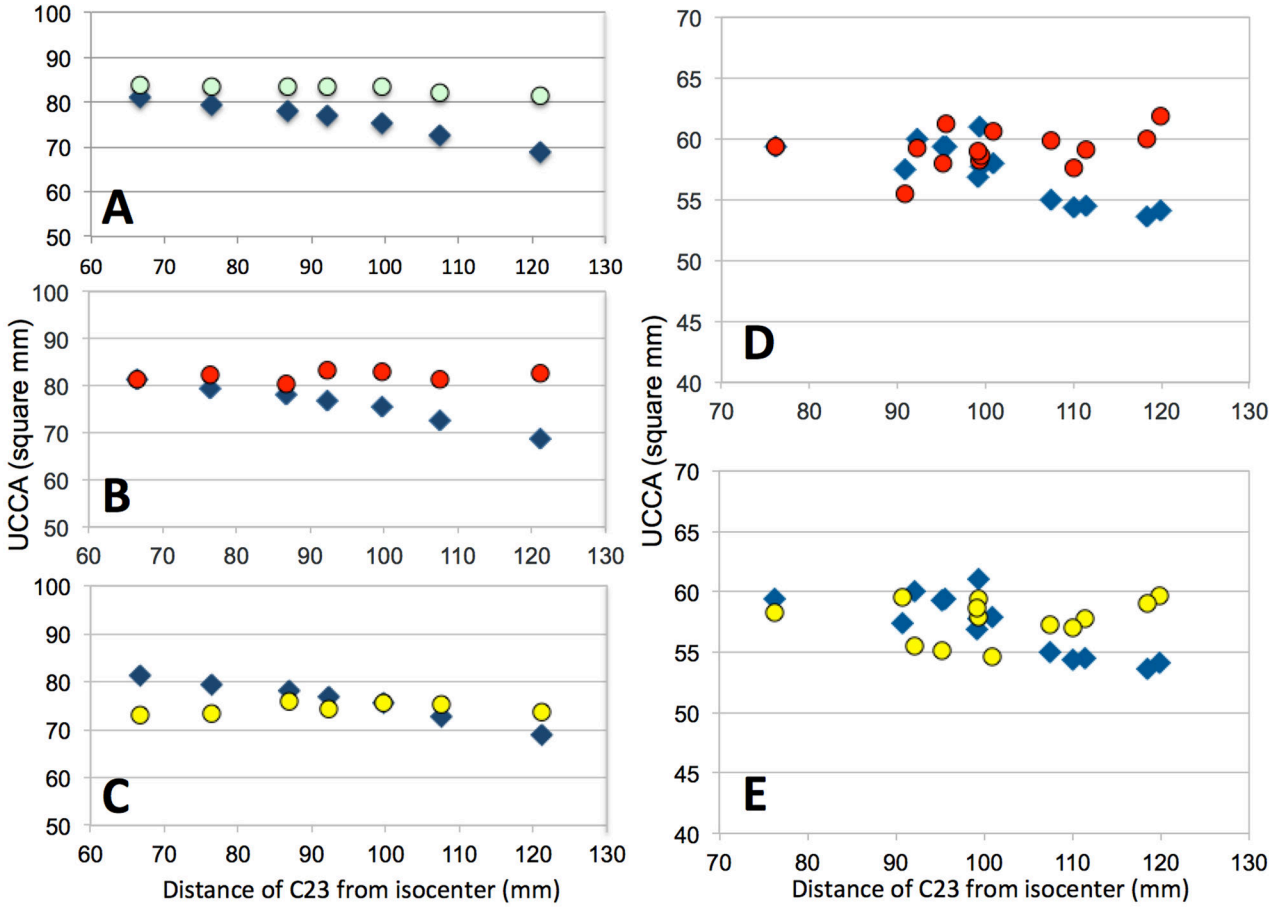

Figure 4.

UCCA as a function of the distance of the C2–3 disc from scanner isocenter: uncorrected data (blue diamonds), retrospectively corrected using the fit of phantom data (emerald circles), normalized using C2 vertebral body diameters (red circles) and normalized using the Jacobian determinant (yellow circles). A, B, C: Healthy control scanned at one site; D, E: multiple sclerosis patient scanned at the 7 NAIMS sites.

Table 1.

Effect of the different correction methods on UCCA measures.

Top row: percent difference of measured UCCA at the extreme table positions (Z_{CImin} and Z_{CImax}). Bottom row: standard deviation of the group of measures performed with different table positions or at the different sites.

Correction method:	None	Scanner 2D	Scanner 3D	Phantom fit	Vertebral diameters	Jacobian
Healthy Control A (single site)	15.2% 4.2mm^2	6.8% 2.0mm^2	2.1% 1.0mm^2	2.9% 0.9mm^2	1.9% 1.1mm^2	0.7% 1.1mm^2
Healthy Control B (single site)	12.0% 3.6mm^2	5.9% 2.0mm^2	1.8% 1.2mm^2	3.2% 1.3mm^2	1.0% 1.9mm^2	–
MS patient (across 7 sites)	9.6% 2.5mm^2	–	–	–	1.1% 1.6mm^2	1.2% 1.7mm^2